



HAL
open science

Dual intra- and extracellular release of monomethyl auristatin E from a neutrophil elastase-sensitive antibody-drug conjugate

Imene Ait Mohamed Amar, Steve Huvelle, Emmanuel Douez, Stéphanie Letast, Sylvain Henrion, Marie-Claude Viaud-Massuard, Nicolas Aubrey, Emilie Allard-Vannier, Nicolas Joubert, Caroline Denevault-Sabourin

► To cite this version:

Imene Ait Mohamed Amar, Steve Huvelle, Emmanuel Douez, Stéphanie Letast, Sylvain Henrion, et al.. Dual intra- and extracellular release of monomethyl auristatin E from a neutrophil elastase-sensitive antibody-drug conjugate. *European Journal of Medicinal Chemistry*, 2022, 229, 11 p. 10.1016/j.ejmech.2021.114063 . hal-03662472

HAL Id: hal-03662472

<https://hal.inrae.fr/hal-03662472v1>

Submitted on 8 Jan 2024

HAL is a multi-disciplinary open access archive for the deposit and dissemination of scientific research documents, whether they are published or not. The documents may come from teaching and research institutions in France or abroad, or from public or private research centers.

L'archive ouverte pluridisciplinaire **HAL**, est destinée au dépôt et à la diffusion de documents scientifiques de niveau recherche, publiés ou non, émanant des établissements d'enseignement et de recherche français ou étrangers, des laboratoires publics ou privés.



Distributed under a Creative Commons Attribution - NonCommercial 4.0 International License

1 **Dual intra- and extracellular release of Monomethyl Auristatin E from**
2 **a neutrophil elastase-sensitive antibody-drug conjugate**

3

4 Imene Ait Mohamed Amar ^{a,1}, Steve Huvelle ^{a,1}, Emmanuel Douez ^b, Stéphanie Letast ^a,
5 Sylvain Henrion ^a, Marie-Claude Viaud-Massuard ^a, Nicolas Aubrey ^c, Emilie Allard-
6 Vannier ^b, Nicolas Joubert ^{a,2,*}, Caroline Denevault-Sabourin ^{a,2,*}.

7

8 ^aEA 7501 GICC, Team IMT, University of Tours, F-37032 Tours, France

9 ^bEA 6295 NMNS, University of Tours, F-37200 Tours, France

10 ^cUMR 1282 ISP, Team BioMAP, University of Tours-INRAE, F-37200 Tours, France.

11 ¹ These authors contributed equally to this work.

12 ² These authors contributed equally to this work.

13

14

15 * Corresponding authors, Innovation Moléculaire et Thérapeutique, EA7501 GICC,
16 University of Tours, UFR de Médecine, Bâtiment Vialle, 7ème étage, 10 Bd Tonnellé,
17 BP 3223, 37032 TOURS Cedex 01, France. Tel.: +33 2 47367231.

18 *E-mail address:* caroline.sabourin@univ-tours.fr (C. Denevault-Sabourin) and
19 nicolas.joubert@univ-tours.fr (N. Joubert).

20

21 **Abstract**

22 Antibody-drug conjugates (ADCs) are targeted therapies, mainly used in oncology,
23 consisting in a three-component molecular architecture combining a highly potent drug
24 conjugated *via* a linker onto a monoclonal antibody (mAb), designed for the selective
25 delivery of the drug to the tumor site. The linker is a key component, defining the ADC
26 stability and mechanism of action, and particularly the drug release strategy. In this
27 study, we have developed and synthesized a cleavable linker, which possesses an Asn-
28 Pro-Val (NPV) sequence sensitive to the human neutrophil elastase (HNE),
29 overexpressed in the tumor microenvironment. This linker permitted the site-specific
30 conjugation of the cell-permeable drug, monomethyl auristatin E (MMAE), onto
31 trastuzumab, using a disulfide re-bridging technology. The resulting ADC was then
32 evaluated *in vitro*. This conjugate demonstrated retained antigen (Ag) binding affinity

33 and exhibited high subnanomolar potency against Ag-positive tumor cells after
34 internalization, suggesting an intracellular mechanism of linker cleavage. While no
35 internalization and cytotoxic activity of this ADC was observed on Ag-negative cells in
36 classical conditions, the supplementation of exogenous HNE permitted to restore a
37 nanomolar activity on these cells, suggesting an extracellular mechanism of drug release
38 in these conditions. This *in vitro* proof of concept tends to prove that the NPV sequence
39 could allow a dual intra- and extracellular mechanism of drug release. This work
40 represents a first step in the design of original ADCs with a new dual intra- and
41 extracellular drug delivery system and opens the way to further experimentations to
42 evaluate their full potential *in vivo*.

43

44 **Keywords**

45 Extracellular release; antibody-drug conjugate (ADC); human neutrophil elastase
46 (HNE); anticancer targeted therapy; cancer; tumor targeting.

47

48 **Abbreviations¹**

49

¹ ADC, antibody-drug conjugate; HNE, human neutrophil elastase; IC₅₀, 50% inhibitory concentration; NPV trigger, asparagine proline. valine trigger;

50 1. Introduction

51

52 Immunoconjugates, and particularly, antibody-drug conjugates (ADCs) have been
53 extensively developed over the last four decades, with applications, mainly in cancer
54 therapy [1,2]. An ADC is a targeted therapy, resulting from the conjugation of a potent
55 agent (also called payload or drug), chemically attached through a linker to a
56 monoclonal antibody (mAb), combining the targeting specificity of the mAb with the
57 high activity of a small molecule drug [3–5]. To date, eleven ADCs have been approved
58 by the Food and Drug Administration (FDA), while around 80 are currently under
59 clinical development [6].

60 The most explored strategy for ADC design consists in cancer cells targeting, using
61 mAb directed against internalizing antigens (Ag) of the cancer cells surface. After
62 specific Ag binding, these conjugates usually undergo an antigen-mediated
63 internalization and release their cytotoxic agent or metabolite in the lysosomal
64 compartment, after, respectively, cleavage of their linker (cleavable linker) or complete
65 ADC digestion (non-cleavable linker) [7].

66 Non-cleavable linkers demonstrate a high plasma stability, but they are also dependent
67 on efficient internalization and intracellular ADC degradation to release an active
68 metabolite [8]. Moreover, due to its charged character at physiological pH, this active
69 metabolite cannot cross biological membranes to achieve a bystander effect on
70 neighboring cells. Therefore, ADCs with non-cleavable linkers lead essentially to the
71 death of Ag-positive tumor cells [9,10]. This strategy, while effective, remains
72 nevertheless restricted to homogeneous tumors, with high level of expression of the
73 targeted Ag. Moreover, the dependence upon direct cell-surface Ag internalization and
74 intracellular processing of these ADCs to be effective make them sensitive to many
75 resistance mechanisms: decrease of target Ag expression, defects in ADC binding,
76 internalization, trafficking or recycling, reduction of lysosomal proteolytic activity, or
77 impaired lysosomal release due to reduced expression of lysosomal transporters [11–
78 16].

79 Cleavable linkers exploit specific features of the tumor endosomal or lysosomal
80 environment (*e.g.* acidic conditions, high glutathione (GSH), glucuronidase or protease
81 levels) for the efficient intracellular release of the free drug (for a review, see [1,7]). The

82 capacity of the released free payload to achieve a bystander killing effect depends on its
83 permeability and its ability to diffuse through biological membranes out of the tumor
84 cell, and enter surrounding cells, leading to death of both Ag-positive and Ag-negative
85 tumor cells [17]. This property permits the treatment of tumors with heterogeneous
86 levels of target Ag expression. Moreover, there is emerging evidence that some of these
87 ADCs with particular cleavable linker/cell-permeable drug combinations can kill cells
88 through mechanisms independently of internalization, and that internalization may be
89 non-essential for their anti-tumor activity [17]. This particularity can be useful to
90 circumvent resistance mechanisms related to ADC endocytosis and intracellular
91 processing. Thus, acid-labile, GSH- or protease (cathepsin B)-sensitive linkers, while
92 being sensitive to tumor lysosomal environment can also be cleaved extracellularly in
93 the tumoral microenvironment [18–25]. Indeed tumoral lysosomal compartment and
94 tumoral microenvironment share characteristic features as acidic pH and high GSH and
95 proteases levels, allowing a dual intra- and extracellular mechanism of release of the
96 active payload from these linkers. In the case of a diffusible drug, the payload
97 extracellularly released can penetrate neighboring cells and achieve bystander tumor
98 cell killing whatever the level of cell target Ag expression and independently of ADC
99 internalization.

100 If acid-labile and GSH-sensitive linkers show limited plasma stability and short half-
101 lives, protease-responsive linkers demonstrate enhanced stability and reduced off-target
102 toxicity and represent an important step in ADC development [26,27]. However,
103 expression, concentration and activity of lysosomal proteases differ between tumors as
104 well as their concentration in the tumor microenvironment [11]. It is consequently
105 worthwhile to widen the scope of protease-sensitive linkers for ADCs.

106 In this context, a tripeptide Asn-Pro-Val (NPV) sequence was identified in 2002, as a
107 specific substrate of human neutrophil elastase (HNE) [28]. HNE is a serine protease,
108 stored in azurophilic granules of neutrophils, which plays a key role in innate immunity
109 and physiologic inflammation [29]. Besides being released in the extracellular space
110 during infection or inflammation, HNE is also secreted by infiltrating neutrophils and
111 granulocytic myeloid derived suppressor cells in the tumor microenvironment,
112 promoting primary tumor growth and secondary organ metastasis. Thus, cancers are
113 characterized by significantly elevated levels of HNE, especially in the stroma [29],

114 which makes HNE an interesting protease for protease-sensitive linkers development.
115 Interesting proofs of concept, using an NPV sequence for the development of original
116 small molecule-drug conjugates (SMDCs), demonstrated that this NPV trigger could be
117 cleaved extracellularly in the presence of HNE. Moreover, these studies showed that
118 this peptide sequence could also be digested by rat-liver lysosome extracts, which can
119 be of interest for a dual intra- and extracellular mechanism of release [30]. To the best
120 of our knowledge, no ADC bearing this sequence have been reported in the literature.
121 These findings prompted us to explore the applicability of NPV linkers in the design of
122 new ADCs. We report herein the development and evaluation of the first HNE-sensitive
123 ADC.

124

125 **2. Results and discussion**

126

127 *2.1. Design of linker-drug*

128

129 In this study, the FDA-approved trastuzumab, which targets the human epidermal
130 growth factor receptor 2 (HER2), was chosen as a model antibody. The linker contains
131 the NPV-PABC-MMAE sequence, with NPV, as the HNE-sensitive trigger, and where
132 the PABC acts as a self-immolative spacer, to free the potent cytotoxic drug
133 monomethyl auristatin E (MMAE), according to the mechanism depicted in Fig. 1.
134 MMAE is able to diffuse through biological membrane, an essential property to achieve
135 a bystander killing effect, necessary in the case of a dual intra- and extracellular
136 mechanism of release. The conjugation of the linker on trastuzumab was realized, by a
137 site-specific conjugation method, using a (diphenylthiomaleimido)caproic acid
138 (diSPhMC) head for disulfide stapling on cysteine residues. This methodology allows
139 the re-bridging of previously reduced interchain disulfide bonds, leading to stable and
140 homogeneous immunoconjugates [31–38], and limiting the formation of low and high
141 DAR species, known to compromise the ADC therapeutic window in auristatin-
142 containing ADCs [39].

143

144 *2.2. Chemistry*

145

146 For the preparation of the linker-drug, the activated site-specific bioconjugation head **2**
147 and the linker-payload fragment **8** were needed. These building blocks were synthesized
148 separately, as described in Scheme 1. The preparation of the 6-(3,4-
149 bis(phenylthio)maleimido)caproic acid **1** was performed according to a previously
150 described literature procedure [35], and then converted into the reactive
151 pentafluorophenyl (Pfp) ester **2**.

152 The synthesis of linker-payload fragment **8** was achieved in five steps from commercial
153 protected amino acids. Briefly, starting from Asn(Trt)-OH, Fmoc-Pro-OH and Fmoc-
154 Val-OH, the tripeptide **3** was easily obtained, using an automated single channel
155 microwave peptide synthesizer. After coupling reaction of intermediate **3** with 4-(((*tert*-
156 butyldimethylsilyl)oxy)methyl)aniline, followed by TBDMS group deprotection, the
157 resulting compound **5** was activated with *p*-nitrophenyl chloroformate to give carbonate
158 **6**. The latter underwent a coupling reaction with MMAE·TFA salt, providing
159 intermediate **7**, which was then deprotected, to remove the Fmoc group, and then
160 coupled with Pfp ester **2**, leading to the desired linker-drug diSPhMC-NPV-PABC-
161 MMAE **9**.

162

163 *2.3. Bioconjugation and characterization of TTZ-MC-NPV-MMAE conjugate*

164

165 The bioconjugation of linker-drug **9** on the internalizing anti-HER2 humanized
166 antibody, trastuzumab (IgG1), was performed in two steps (Fig. 1). Interchain disulfide
167 bridges of trastuzumab were first mildly reduced, using 6 eq of tris(2-
168 carboxyethyl)phosphine (TCEP) to release the free thiols, and then 6 eq of compound **9**
169 were added to bridge the cysteine residues. This sequence was repeated, using 3 eq of
170 TCEP and linker-drug **9**. The mixture was finally purified by size-exclusion
171 chromatography on a Superdex 75 column, leading to TTZ-MC-NPV-MMAE (**10**).

172 The characterization of TTZ-MC-NPV-MMAE **10** was realized by denaturing high-
173 resolution mass spectrometry (HRMS) (Supporting Information Fig. S1). The drug-to-
174 antibody ratio (DAR) of conjugate **10** was then determined by HRMS (Supporting
175 Information Fig. S1) and by hydrophobic interaction chromatography (HIC)
176 (Supporting Information Fig. S2). Both methods demonstrated an average DAR of 3.5,
177 with, in HIC, more than 50% of DAR 4 species, an optimal DAR for MMAE-containing

178 ADCs [39,40]. As expected when performing disulfide stapling with a bioconjugation
179 head, unconjugated mAb (DAR 0) or species with high DAR (> 5) were not observed.
180 Finally, the aggregation profile of conjugate **10** was studied by size-exclusion
181 chromatography (SEC). These data revealed no obvious aggregation and suggested that
182 TTZ-MC-NPV-MMAE was composed of more than 91% of monomer (Supporting
183 Information Fig. S3).

184

185 *2.4. Binding affinity of TTZ-MC-NPV-MMAE conjugate*

186

187 In order to test whether our new linker affected antigen recognition, the HER2 binding
188 properties of TTZ-MC-NPV-MMAE (**10**) was then evaluated by enzyme-linked
189 immunosorbent (ELISA) assay in comparison to the non-conjugated native antibody,
190 trastuzumab. The ADC **10** was found to have retained binding to HER2, which was
191 comparable to trastuzumab (Fig. 2). These dose-response experiments showed that the
192 MC-NPV-MMAE linker-drug had a minimal impact on antigen recognition.

193

194 *2.5. Enzymatic cleavage of TTZ-MC-NPV-MMAE conjugate*

195

196 The enzymatic cleavage of TTZ-MC-NPV-MMAE (**10**) in presence of HNE was further
197 evaluated, using denaturing mass spectrometry for samples analysis. Quantitative NPV
198 linker cleavage was observed within 2 h (Supporting Information Fig. S4), confirming
199 that our new linker was cleaved by the enzyme. The subsequent MMAE release from
200 the linker in presence of HNE was then studied, using high performance liquid
201 chromatography (HPLC) for analysis. On HNE addition, the NPV linker was cleaved
202 and only free MMAE was observed, which indicates both cleavage and efficient self-
203 immolation of the PABC unit (Supporting Information Fig. S5).

204

205 *2.5. Internalization of TTZ-MC-NPV-MMAE conjugate*

206

207 The internalization of TTZ-MC-NPV-MMAE (**10**) was then evaluated by confocal
208 fluorescence microscopy and flow cytometry studies (FACS analysis) on two human
209 cell lines: SK-BR-3, a HER2 overexpressing breast cancer cell line (HER2+), and

210 MDA-MB-231, a highly aggressive triple-negative breast cancer (TNBC) cell line,
211 characterized by a lack of HER2 gene amplification (HER2-). As shown in Fig. 3, after
212 48 h of exposure, a fair accumulation of ADC **10** in the intracellular compartments of
213 HER2-positive SK-BR-3 cells was detected, suggesting an efficient receptor-mediated
214 endocytosis of ADC **10** in these cells (Fig. 3A). On the contrary, no significant
215 intracellular uptake was observed in HER2-negative MDA-MB-231 cells (Fig. 3B).
216 Moreover, a quantitative evaluation of endocytosis was performed by flow cytometry
217 after the pre-incubation of ADC **10** with protein L coupled with phycoerythrin (ppL-
218 PE), used as an intracellular tracer (Fig. 3C). The non-specific uptake of ppL-PE has
219 been quantified and was considered negligible regarding the obtained values (28
220 arbitrary units (AU) for SK-BR-3 HER2+ cells *versus* 14 AU for MDA-MB-231 HER2-
221 cells). Results showed that there is a large increase of the uptake of ADC **10** on HER2+
222 cancer cells compared to HER2- cells as the mean fluorescence intensity (MFI) increase
223 from 16 to 250 on MDA-MB-231 and SK-BR-3 cell lines, respectively. The presence of
224 HNE do not alter this entry as the MFI are unchanged for the cells incubated with ADC
225 **10** in the presence of the enzyme.

226

227 *2.6. In vitro antitumor activity of TTZ-MC-NPV-MMAE conjugate*

228

229 Antiproliferative activity of TTZ-MC-NPV-MMAE (**10**) was then tested *in vitro*, in
230 presence or absence of HNE supplementation in the culture medium at a nontoxic
231 concentration (50 nM), on SK-BR-3 (HER2+) and MDA-MB-231 (HER2-) cell lines.
232 Cytotoxic effects were evaluated using a luminescent CellTiter-Glo proliferation assay,
233 based on ATP quantification (Promega Wiscousin, USA) [41]. Trastuzumab and free
234 MMAE were used as controls.

235 As shown in Table 1, in absence of HNE supplementation, ADC **10** demonstrated a
236 highly potent cytotoxic activity on HER2+ SK-BR-3 cells (IC₅₀ of 0.23 ± 0.08 nM)
237 (Table 1, entry 1), in which a massive intracellular ADC uptake was detected,
238 suggesting an intracellular mechanism of linker cleavage. These results are consistent
239 with the literature data [30] that reported evidence of NPV linker digestion by lysosome
240 extracts, permitting the intracellular lysosomal cleavage of the NPV linker after ADC
241 internalization (Fig. 5).

242 The addition of HNE in the culture medium led to a very similar cell proliferation
243 inhibition profile of ADC **10** on SK-BR3-cells (Fig. 4 and Table 1, entry 2), suggesting
244 that the possibility of a dual intra- and extracellular mechanism of release does not
245 affect the global activity of ADC **10** on Ag-positive tumor cells.

246 In absence of HNE supplementation, ADC **10** did not display significant cytotoxicity on
247 HER2- MDA-MB-231 cells ($IC_{50} > 1000$ nM), whereas free MMAE inhibited cell
248 proliferation at subnanomolar concentrations (IC_{50} of 0.53 ± 0.06 nM) (Table 1, entries
249 1 and 4). These results demonstrated that, without HNE addition, ADC **10** is inactive on
250 target Ag-negative tumor cells, where no ADC internalization by receptor-mediated
251 endocytosis was observed, tending to prove that, in these conditions, neither intra- nor
252 extracellular linker cleavage can occur to release the free MMAE.

253 In contrast, after addition of exogenous HNE, ADC **10** significantly inhibited MDA-
254 MB-231 cell growth at nanomolar concentrations (IC_{50} of 47.5 ± 7.9 nM) (Table 1, entry
255 2), suggesting an extracellular cleavage of the HNE-sensitive linker, followed by
256 passive diffusion of the free MMAE released, across the cell membrane of neighboring
257 cells, allowing a cytotoxic activity on these Ag-negative cancer cells (Fig. 5).

258

259 **3. Conclusion**

260

261 In the course of ADCs development, the nature of the linker, connecting the highly
262 potent drug to the mAb is a key component to consider, requiring careful design. The
263 emergence of protease-sensitive linkers has revolutionized this field of research,
264 enhancing linker stability and cleavage selectivity to improve ADC therapeutic index.
265 One of the well-established hallmarks of cancers is the presence of an inflammatory
266 microenvironment associated with tumor-infiltrating immune cells, secreting high levels
267 of proteases [42], such as HNE, which can be exploited to trigger a selective drug
268 release in the tumor microenvironment. In this study, we used the HNE-sensitive NPV
269 sequence to design an ADC with a new dual intra- and extracellular drug delivery
270 system. This ADC was able to kill Ag-positive tumor cells after internalization with
271 IC_{50} in the subnanomolar range. While no internalization and cytotoxic activity of this
272 ADC was observed on Ag-negative cells in classical conditions, the addition of
273 exogenous HNE, known to be overexpressed in the tumor microenvironment, permitted

274 to restore a nanomolar activity on these cells, suggesting an extracellular mechanism of
275 drug release in these conditions, and a subsequent bystander killing effect. These studies
276 tend to prove that the NPV sequence could allow a dual intra- and extracellular
277 mechanism of drug release, which could be of great interest in heterogeneous tumors
278 with various levels of cell target Ag expression or to circumvent some issues related to
279 the dependence of ADCs upon cell-surface Ag internalization and intracellular
280 processing. Moreover, the diffusion of the free cytotoxic drug released in the tumor
281 microenvironment could trigger the death of a large variety of Ag-negative tumor cells
282 or cancer-associated cells, like tumor endothelial cells, which may be of interest in the
283 field of cancer therapy. This *in vitro* proof of concept remains to be confirmed *in vivo* in
284 mouse models. As high levels of HNE are observed in many cancers, we believe that
285 this strategy could be applied in the design of ADCs directed against a great variety of
286 tumor types.
287

288 5. Experimental section

289

290 5.1. General remarks

291

292 All solvents were anhydrous reagents from commercial sources. Unless otherwise
293 noted, all chemicals and reagents were obtained commercially and used without
294 purification. TFA salt of MMAE was purchased from Levena Biopharma (#T1004).

295 Known compounds were prepared according to literature procedures: 4-(((*tert*-
296 butyldimethylsilyl)oxy)methyl)aniline [43], compound **1** [35].

297 Trastuzumab (Ontruzant[®], Samsung Bioepis) was kindly provided by the Hospital
298 Pharmacy of the Tours Teaching Hospital.

299 Microwave heating and peptide synthesis were carried out with a single-mode Initiator
300 Alstra unit (Biotage). Thin layer chromatography (TLC) was performed using
301 commercial pre-coated aluminium sheets silica gel (60 Å, F254; Merk) and revealed
302 under 254 nm UV lamp. Column chromatography was carried out on an ISCO
303 purification unit, Combi Flash RF 75 PSI, with Redisep flash silica gel columns (60 Å,
304 230-400 mesh, grade 9385). Purity of final compounds was determined by high
305 performance liquid chromatography (HPLC). HPLC analysis were carried out with a
306 LaChrom Elite system [Hitachi L-2130 (pump), L-2200 (autosampler) and L-2400 (UV-
307 detector)], with a UV detection at 254 nm at 25 °C, and a XBridge C-18 column (250 ×
308 10 mm, 4 µm, 135 Å); elution was performed with 0.1% trifluoroacetic acid (TFA) in
309 water (solvent A), and 0.1% TFA in acetonitrile (MeCN) (solvent B), with a gradient
310 from 20 to 100% of B over 35 minutes with a flow rate of 1 mL.min⁻¹; injection was
311 realized at 1 mg/mL in DMSO (10 µL). Final compounds were obtained in a purity ≥
312 95%. Semi-preparative HPLC was carried out on a Gilson PLC 2050 system [ARMEN
313 V2 (pump), ECOM TOYDAD600 (UV-detector)], with a UV detection at 254 nm at 25
314 °C, and a Waters XBridge[™] C-18 column (250 mm x 19 mm, 5 µm); elution was
315 performed with 0.1 % TFA in water (solvent A), and 0.1% TFA in MeCN (solvent B);
316 with a gradient from 20 to 100% of B over 32 min and then 100% of B for 6 min at 17.1
317 mL/min. NMR spectra were recorded at 300 MHz (¹H) on a Bruker Avance (300 MHz)
318 spectrometer, and at 400 MHz (¹H) on a Bruker AVANCE NEO (400 MHz)
319 spectrometer. The chemical shifts are reported in parts per million (ppm, δ) relative to

320 residual deuterated solvent peaks. The abbreviations s = singlet, d = doublet, t = triplet,
321 q = quadruplet, m = multiplet and bs = broad signal were used throughout.

322 For small-molecule mass analysis, high-resolution accurate mass spectrometry
323 measurements (HRMS) were performed using an Acquity UPLC H-Class system
324 hyphenated to a Vion IMS Q-ToF mass spectrometer (Waters). Before MS analysis, 1 ng
325 of sample was injected onto a BEH C18 column (2.1 × 50 mm, 1.7 μm) heated to 50 °C.
326 A 6 min gradient from 5% to 90% solvent B was applied with a 0.5 mL/min flow rate to
327 elute the sample (solvent A: H₂O + 0.1% formic acid; solvent B: MeCN + 0.1% formic
328 acid). MS data were acquired in positive mode with an ESI source over a 50-1400 *m/z*
329 window with 0.2 Hz scan rate and collision energy ramp from 20 to 40 eV. Data were
330 processed using UNIFI software version 1.9.4.

331

332 5.2. Chemistry

333

334 5.2.1. Perfluorophenyl 6-(3,4-bis(phenylthio)maleimido)hexanoate (**2**)

335 6-(3,4-bis(phenylthio)maleimido)caproic acid (46.6 mg, 0.11 mmol) and
336 pentafluorophenol (20.1 mg, 0.11 mmol) were dissolved in 1.5 mL of dry
337 tetrahydrofuran (THF) and stirred at ice bath temperature. *N,N'*-
338 dicyclohexylcarbodiimide (DCC) (22.5 mg, 0.11 mmol) was then added to the solution
339 at 0 °C. The resulting mixture was stirred overnight at room temperature. The solvent
340 was then removed under reduced pressure, and the residue was dissolved in
341 dichloromethane (DCM) and filtrated. The crude was finally purified by column
342 chromatography using cyclohexane with ethyl acetate gradient (0-10%) as eluent to
343 afford compound **2** (58.6 mg, 91%) as a yellow oil.

344 ¹H NMR (300 MHz, CDCl₃) δ 7.38-7.22 (m, 10H), 3.57 (t, 2H, *J* = 7.5 Hz), 2.69 (t, 2H,
345 *J* = 7.5 Hz), 1.82 (dt, 2H, *J* = 15.0, 7.5 Hz), 1.69 (dt, 2H, *J* = 15.0, 7.5 Hz), 1.50-1.30
346 (m, 2H). HRMS (ESI) *m/z*: [M+H]⁺ calcd for C₂₈H₂₁F₅NO₄S₂, 594.0827; found
347 594.0823.

348

349 5.2.2. Fmoc-Asn-Pro-Val-OH (**3**)

350 Into a specific microwave vial was introduced a Fmoc-Val-OH loaded Wang resin (700
351 mg, 0.7 mmol/g, 0.49 mmol). The resin was activated by DCM (32 mL) and the solvent

352 was removed by filtration. Then, piperidine (11.5 mL, 20% in DMF) was introduced.
353 The suspension was shaken smoothly at room temperature and filtrated to give the
354 deprotected Val-OH loaded on resin. Then, *N,N'*-diisopropylcarbodiimide (DIC) (353.5
355 μL , 1.96 mmol), Oxyma (310.5 mg, 1.96 mmol, 4.5 M in *N*-methyl-2-pyrrolidone) and
356 Fmoc-Pro-OH (685 mg, 1.96 mmol, 0.7 M in *N,N*-dimethylformamide (DMF)) were
357 introduced and the mixture was stirred at 70 °C for 30 min. The resin was washed with
358 DMF and deprotection and coupling procedures were repeated with Asn(Trt)-OH (596.7
359 mg, 1.21 mmol, 0.7 M in DMF) to afford the resin-grafted tripeptide. The resin was
360 washed with methanol and was treated with a TFA/H₂O/TIPS mixture (95/2.5/2.5, 7.55
361 mL) for 2 h at room temperature. Resin was filtrated and the filtrate was concentrated
362 under reduced pressure. The residue was dissolved in acetone (10 mL) and precipitated
363 with diethyl ether (50 mL) to afford the tripeptide **3** (222 mg, 82%), as a white solid.
364 ¹H NMR (400 MHz, DMSO-*d*₆) δ 12.49 (s, 1H), 7.92 (dd, 2H, *J* = 23.0, 7.5 Hz), 7.68
365 (dd, 2H, *J* = 23.0, 7.5 Hz), 7.36 (ddd, 4H, *J* = 23.0, 15.0, 7.5 Hz), 7.25-7.07 (m, 1H),
366 6.92 (s, 1H), 4.61 (dd, 1H, *J* = 15.0, 7.5 Hz), 4.44 (d, 1H, *J* = 7.5 Hz), 4.31-4.15 (m,
367 2H), 4.07 (dd, 1H, *J* = 8.0, 6.2 Hz), 3.60-3.27 (m, 5H), 2.47-2.29 (m, 2H), 2.03 (ddd,
368 2H, *J* = 23.0, 15.0, 8.0 Hz), 1.87 (d, 2H, *J* = 4.1 Hz), 1.06-0.79 (m, 6H). HRMS (ESI)
369 *m/z*: [M+H]⁺ calcd for C₂₉H₃₅N₄O₇, 551.2500; found, 551.2494.

370

371 5.2.3. Fmoc-Asn-Pro-Val-PAB-OH (**5**)

372 To a solution of compound **3** (198 mg, 0.36 mmol) in dry DCM (2.5 mL) at 0 °C, under
373 an argon atmosphere, were added DCC (111 mg, 0.54 mmol) and a catalytic amount of
374 4-dimethylaminopyridine (DMAP). The resulting mixture was stirred 1 h at 0 °C and 4-
375 (((*tert*-butyldimethylsilyl)oxy)methyl)aniline (85 mg, 0.36 mmol) was added. The
376 suspension was stirred overnight at room temperature, filtered on a celite pad,
377 concentrated and purified by silica column chromatography using DCM with methanol
378 (MeOH) gradient (0-8%) as eluent, to give intermediate **4** (167 mg, 60%) as a yellow oil
379 (HRMS (ESI) *m/z*: [M+Na]⁺ calcd for C₄₂H₅₅N₅NaO₇Si, 792.3769; found, 792.3767).
380 To a solution of intermediate **4** (167 mg, 0.22 mmol) in absolute ethanol (2 mL) was
381 added 20 μL of concentrated HCl (37% w/w). The resulting mixture turned red
382 immediately and was stirred 2 h at room temperature. The solvent was then removed
383 under reduced pressure, and the residue was finally purified by column chromatography

384 using DCM with MeOH gradient (0-10%) as eluent, to give compound **5** (132 mg, 92%,
385 55% over two steps) as an off-white powder.

386 ¹H NMR (400 MHz, CDCl₃) δ 8.60 (s, 1H), 7.75 (d, 2H, *J* = 7.5 Hz), 7.59-7.47 (m, 5H),
387 7.42-7.28 (m, 4H), 7.20 (d, 2H, *J* = 7.5 Hz), 6.26-5.99 (m, 2H), 4.74-3.84 (m, 10H),
388 2.80-2.65 (m, 1H), 2.55-2.42 (m, 1H), 2.25-1.95 (m, 7H), 0.98 (dd, 6H, *J* = 14.0, 6.6
389 Hz). HRMS (ESI) *m/z*: [M+H]⁺ calcd for C₃₆H₄₂N₅O₇, 656.3084; found, 656.3067.

390

391 5.2.4. Fmoc-Asn-Pro-Val-PABC-PNP (**6**)

392 A mixture of compound **5** (26.1 mg, 0.04 mmol), *para*-nitrophenyl chloroformate (16.1
393 mg, 0.08 mmol), and dry pyridine (8.0 μL, 0.10 mmol) in dry THF (2 mL), under an
394 argon atmosphere, was stirred overnight at room temperature. The solvent was then
395 removed under reduced pressure, and the residue was finally purified by column
396 chromatography using DCM with MeOH gradient (0-8%) as eluent, to give
397 intermediate **6** (31.4 mg, 96%) as an orange solid.

398 ¹H NMR (300 MHz, CDCl₃) δ 8.95 (s, 1H), 8.29-8.17 (m, 2H), 7.74 (d, 2H, *J* = 6.0 Hz),
399 7.66 (d, 2H, *J* = 6.0 Hz), 7.56 (dd, 2H, *J* = 6.0, 3.0 Hz), 7.47-7.23 (m, 8H), 6.30 (s, 1H),
400 6.17 (d, 1H, *J* = 9.0 Hz), 5.62 (s, 1H), 5.21 (s, 2H), 4.90-4.72 (m, 1H), 4.70-4.50 (m,
401 1H), 4.45-4.10 (m, 4H), 3.78 (t, 2H, *J* = 6.0 Hz), 2.90-2.71 (m, 1H), 2.66-2.50 (m, 1H),
402 2.41-2.19 (m, 2H), 2.15-1.75 (m, 4H), 0.95 (dd, 6H, *J* = 21.0, 6.0 Hz). HRMS (ESI)
403 *m/z*: [M+Na]⁺ calcd for C₄₃H₄₄N₆O₁₁Na 843.2966; found 843.2955.

404

405 5.2.5. Fmoc-Asn-Pro-Val-PABC-MMAE (**7**)

406 To a solution of compound **6** (25 mg, 0.03 mmol), hydroxybenzotriazole (HOBt) (14
407 mg, 0.10 mmol) and *N,N'*-diisopropylethylamine (DIPEA) (10.4 μL, 0.06 mmol) in dry
408 DMF (1 mL), under an argon atmosphere, was added the trifluoroacetic salt of MMAE
409 (15 mg, 0.02 mmol) in solution in dry DMF (1 mL). The resulting mixture was stirred
410 overnight at room temperature and purified by semi-preparative HPLC (0.1% TFA,
411 H₂O/ACN 80/20 method) to give intermediate **7** (20.4 mg, 48%) as a white solid.

412 ¹H NMR (300 MHz, CDCl₃) δ 8.46 (bs, 1H), 7.90-7.65 (m, 4H), 7.63-7.22 (m, 2H),
413 7.49-7.27 (m, 11H), 6.70-3.69 (m, 16H), 3.64-1.45 (m, 39H), 1.35-1.10 (m, 4H), 1.08-
414 0.42 (m, 29H). HRMS (ESI) *m/z*: [M+H]⁺ calcd for C₇₆H₁₀₇N₁₀O₁₅, 1399.7917; found,
415 1399.7870.

416

417 *5.2.6. diSPhMC-Asn-Pro-Val-PABC-MMAE (9)*

418 To a solution of compound **7** (20 mg, 0.014 mmol) in dry DMF (800 μ L) was added
419 piperidine (200 μ L). The resulting mixture was stirred 1 h at room temperature and
420 purified by semi-preparative HPLC (0.1% TFA, H₂O/ACN 80/20 method) to give a
421 mixture of compound **8** (6.0 mg estimated by NMR; HRMS (ESI) *m/z*: [M+2H]²⁺ calcd
422 for C₆₁H₉₈N₁₀O₁₃, 589.3658; found, 589.3655) inseparable from a TFA salt of
423 piperidine. A mixture of compound **8** (6 mg, 0.005 mmol), intermediate **2** (2.8 mg,
424 0.005 mmol), HOBt (1.3 mg, 0.010 mmol) and DIPEA (1.74 μ L, 0.011 mmol) in dry
425 DMF (700 μ L), under an argon atmosphere, was stirred overnight at room temperature.
426 The resulting solution was then purified by semi-preparative HPLC (0.1% TFA,
427 H₂O/ACN 80/20 method) to give linker-drug **9** (6.8 mg, 30% over two steps) as a
428 yellow solid.

429 ¹H NMR (300 MHz, DMSO-*d*₆) δ 9.93 (s, 1H), 8.43-6.86 (m, 26H), 5.37 (dd, 2H, *J* =
430 21.0, 6.0 Hz), 5.14-3.52 (m, 20H), 3.26-2.70 (m, 15H), 2.19-0.65 (m, 51H). HRMS
431 (ESI) *m/z*: [M+Na]⁺ calcd for C₈₃H₁₁₅N₁₁NaO₁₆S₂, 1608.7862; found, 1608.7944.

432

433 *5.3. Antibody conjugation, TTZ-MC-NPV-MMAE (10)*

434

435 Into three vials, were added trastuzumab (4.8 mg/mL, 500 μ L) in BBS buffer (pH 8) and
436 TCEP (97 μ L, 6 eq, 1 mM in BBS buffer) and the reaction was incubated for 1.25 h at
437 37 °C. Linker **9** (97 μ L, 6 eq, 1 mM in DMSO) was then added, and the reaction was
438 incubated for 16 h at 4 °C under agitation (600 rpm). A second addition of TCEP (48
439 μ L, 3 eq, 1 mM in BBS buffer) was performed and the reaction was incubated for 1.25 h
440 at 37 °C. A second addition of the linker **9** (48 μ L, 3 eq, 1 mM in DMSO) was
441 performed, and the reaction was incubated for 22 h at 4 °C under agitation (600 rpm).
442 The mixture was finally purified by size-exclusion chromatography (SEC) on a
443 Superdex[®] 200 10/300 GL column (1.0 x 300 mm, 13 μ M, molecular mass range 10,
444 000 - 600,000 Da) from Cytiva (GE Healthcare Life Sciences, 17-5174-01), connected
445 to an Äkta purifier (Cytiva). The column was used at a rate of 0.8 mL/min with a UV
446 detector at 280 nm. After the loading of TTZ-MC-NPV-MMAE, the column was eluted

447 with PBS for 0.2 column volume (cv), then with 0.3 cv of H₂O/ACN (7/3) + 0.2% TFA
448 and finally with PBS (1 cv) to give TTZ-MC-NPV-MMAE (**10**) (4.8 mg, 67%).

449

450 5.4. ADC Analysis

451

452 5.4.1. Denaturing High-Resolution Mass Spectrometry

453 Denaturing high-resolution mass spectrometric analysis of ADCs were performed on a
454 Bruker maXis mass spectrometer coupled to a Dionex Ultimate 3000 RSLC system.
455 Prior to MS analysis, samples (ca. 5 µg) were desalted on a MassPREP desalting
456 cartridge (2.1 × 10 mm, Waters) heated at 80 °C using 0.1% formic acid as solvent A
457 and 0.1% formic acid in MeCN as solvent B at 500 µL/min. After 1 min, a linear
458 gradient from 5 to 90% B in 1.5 min was applied; the first 1.5 min were diverted to
459 waste. HRMS data were acquired in positive mode with ESI source over the *m/z* range
460 from 900 up to 5000 at 1 Hz and processed using DataAnalysis 4.4 software (Bruker)
461 and the MaxEnt algorithm for spectral deconvolution. Deconvolution was carried out in
462 the range 20-180 kDa, with results recorded for full antibody (LHHL) and for fragments
463 L, LH, HH, LHH (obtained from antibody dissociation during analysis). The average
464 drug-to-antibody ratio (DAR) was calculated as an average of the percentage abundance
465 of each present DAR species, with the quantities calculated by peak integration of the
466 first glycosylation peak, following the corresponding formula:

$$467 \quad DAR_{average} = \frac{DAR_{LHHL} + (DAR_{LHH} + DAR_L) + (2 * DAR_L + 2 * DAR_H) + 2 * DAR_{LH}}{4}$$

468

469 5.4.2. Hydrophobic Interaction Chromatography (HIC) analysis

470 TTZ-MC-NPV-MMAE (**10**) was diluted to 1 mg/mL in PBS pH 7.4 and filtered on a
471 0.22 µm PVDF membrane. Then 50 µg of the sample was injected on a MAbPac HIC-
472 Butyl (4.6 × 100 mm, 5 µm) from Thermo Scientific, connected to a Waters Alliance
473 (e2695) apparatus equipped with a photodiode array detector (2998) set for detection at
474 280 nm. Samples were run with a linear gradient from 100% buffer A (1.5 M
475 ammonium sulfate, 50 mM sodium phosphate, 5% 2-propanol (v/v), pH 7.0) to 20%
476 buffer B (50 mM sodium phosphate, 20% 2-propanol (v/v), pH 7.0) over 2 min and then
477 to 85% buffer B over 30 min and held for 1 min at a flow rate of 1 mL/min. The column
478 oven temperature was maintained at 25 °C. The drug-loaded species are resolved by

479 HIC based on the increasing hydrophobicity. The least hydrophobic and unconjugated
480 form eluted first, while the most conjugated and hydrophobic form eluted last. The area
481 percentage of each peak DAR_i represents the relative distribution of each particular
482 drug-loaded ADC species. The weighted average DAR was then calculated using the
483 percentage peak areas combined with their respective drug load numbers, according to
484 the corresponding formula:

$$485 \quad DAR_{average} = 0 * DAR_0 + 1 * DAR_1 + 2 * DAR_2 + 3 * DAR_3 + 4 * DAR_4 + 5 * DAR_5$$

486

487 *5.4.3. Size-Exclusion Chromatography (SEC) Analysis*

488 ADCs were diluted to 1 mg/mL with PBS pH 7.4 and filtered on a 0.22 μ m PVDF
489 membrane. A sample of 40 μ g was injected on an AdvanceBio SEC (7.8 \times 300 mm, 2.7
490 μ m) from Agilent Technologies, connected to a Waters Alliance (e2695) apparatus
491 equipped with a photodiode array detector (2998) set for detection at 280 nm. Samples
492 were run with an isocratic gradient (1 mM potassium phosphate monobasic, 155 mM
493 sodium chloride, 3 mM sodium phosphate dibasic, 3 mM sodium azide, pH 7.0) over 24
494 min at a flow rate of 1 mL/min. The column oven temperature was maintained at 25 $^{\circ}$ C.

495

496 *5.5. Biology*

497

498 *5.5.1. ELISA assays*

499 HER2 recombinant protein (Sino Biologicals, Beijing, P. R. China) was coated in a 96-
500 well plates at 1 μ g.mL⁻¹ in PBS and incubated overnight at 4 $^{\circ}$ C. The wells were then
501 saturated with 3% BSA-PBS for 1 h at 37 $^{\circ}$ C, and washed with PBS prior to incubation
502 with PBS (negative control), ADCs or trastuzumab (Ontruzant[®], MSD laboratory,
503 France) from 0.001 to 300 μ M during 1 h at 37 $^{\circ}$ C. Wells were then washed with PBS-
504 Tween 20 (0.05%) and incubated with 100 μ L of protein-L-peroxydase
505 (ThermoScientific, Pierce[®], Massachusetts, USA) at 1.25 μ g.mL⁻¹ for 1 h at 37 $^{\circ}$ C, and
506 100 μ L of 3,3',5,5'-tetramethylbenzidine substrate (TMB) (Sigma, St Louis, USA) were
507 added in each well. Enzymatic reactions were stopped with the addition of 50 μ L of 1 M
508 H₂SO₄ and the absorbance was measured at 450 nm, using an absorbance microplate
509 reader (Bio-Tek[®] instruments, Inc., Vermont, USA).

510

511 5.5.2. *Enzymatic Cleavage Assays*

512 HNE (#324681, Sigma-Aldrich) was diluted to 50 µg/mL in 0.1 M Tris-HCl pH 8.0.
513 The cleavage of NPV linker was first realized. The reactivity of the
514 diphenylthiomaleimide scaffold of linker **9** prevented its use in this biochemical
515 cleavage test; the NPV-containing intermediate **8** was thus evaluated. The enzyme
516 substrate MeO-Suc-Ala-Ala-Pro-Val-pNA (#M4765, Sigma-Aldrich) was used as
517 positive control to validate HNE activity. A solution of compound **8** or MeO-Suc-Ala-
518 Ala-Pro-Val-pNA (9 µL of a 2 mM solution in DMSO), Tris-HCl 0.1 M pH 8.0 (49 µL)
519 and HNE (2 µL), for conditions with HNE, or Tris-HCl 0.1 M pH 8.0 (2 µL), for
520 conditions without HNE, was incubated for 24 h at 37 °C. Samples were then analyzed
521 by HPLC with a UV detection at 254 nm (for MeO-Suc-Ala-Ala-Pro-Val-pNA) or at
522 215 nm for the MMAE-containing compound **8**. Elution was performed with 0.1% TFA
523 in water (solvent A), and 0.1% TFA in MeCN (solvent B), with a gradient from 20 to
524 100% of B over 32 min and then 100% of B for 6 min at 17.1 mL/min.
525 For the cleavage of the whole ADC **10** experiment, a 6 µM solution in PBS (pH 7.4) of
526 conjugate **10** was incubated at 37 °C for 2 h with HNE (0.15 µM) or without HNE.
527 Samples were analyzed by denaturing mass spectrometry (*cf.* 5.4.1).

528

529 5.5.3. *Confocal Fluorescence Microscopy*

530 Protein L coupled with phycoerythrin (ppL-PE, Sinobiological, *Beijing, China*) was
531 used as an intracellular tracer. Protein L was obtained from *Peptostreptococcus magnus*.
532 This protein possesses a high affinity for kappa light chain of anti-HER2-like
533 antibodies. Briefly, 30,000 SK-BR-3 and MDA-MB-231 cells were seeded 48 h on p-D-
534 lysine coated glass slides. ADCs were then incubated 30 minutes with ppL-PE in a 1:2
535 ratio at 37 °C, and 10 nmol/L of ADC-ppL-PE complexes were incubated on cells for
536 48 h. Cells were washed three times with cold PBS. Finally, glass slides were assembled
537 on the reverse side with a mounting medium, Fluoromount-G (Thermofisher, Waltham
538 MA, USA). Observations were carried out on a fluorescence confocal microscope
539 (Leica SP8 Confocal Microscope, Leica Microsystems, Nanterre, France) with a x63
540 objective lens and a white light laser (Leica). Images were analyzed by Leica
541 Application Suite X software.

542

543 *5.5.4. Flow Cytometry Studies*

544 Briefly, 50,000 SK-BR-3 and MDA-MB-231 cells were seeded 24 h on 24-well plates.
545 ADCs were then incubated 30 minutes with ppL-PE (1:2 ratio) at 37 °C, and 10 nmol/L
546 of ADC-ppL-PE complexes were incubated on cells with or without elastase enzyme for
547 48 h. Cells were then washed three times with cold PBS, and transferred on 96 round
548 bottom wells plates in a PBS, BSA 1% and EDTA 2 mM solution. Finally, cells were
549 analyzed by a MACSQuant 10 flow cytometer (Miltenyi Biotec) with an excitation laser
550 at 488 nm (filter 565-605 nm) to detect PE fluorescence.

551

552 *5.5.5. Cell Cultures and Reagents*

553 MDA-MB-231 human breast carcinoma cells were obtained from the American Type
554 Culture Collection (LGC Promochem, Molsheim, France). The cells were cultured in
555 Dulbecco's Modified Eagle Medium (DMEM), with 10% fetal bovine serum (FBS,
556 Gibco®), glucose, L-glutamine, and 1% Penicillin-Streptomycin solution (10,000 U/mL,
557 Gibco®) at 37 °C and 5% CO₂. SK-BR-3 cell lines were obtained from Cell Lines
558 Service (CLS Eppelheim, Germany). SK-BR-3 cells were maintained in DMEM
559 supplemented with 10% FBS and 1% Penicillin-Streptomycin solution, in humidified
560 atmosphere at 37 °C with 5% CO₂.

561

562 *5.5.6. Cell Proliferation Assays*

563 Cell viability and proliferation were studied, using a luminescent test based on
564 quantification of ATP, using the CellTiter-Glo cell proliferation assay (Promega
565 Wiscousin, USA). Briefly, 6.000 SK-BR-3 cells or 3.000 MDA-MB-231 cells were
566 incubated in 100 µL of medium in 96-well plates for 24 h and then treated with
567 concentrations ranging from 0.001 nM to 1000 nM of tested compounds. For the
568 conditions with elastase, 50 µL of medium were removed and HNE (#324681, Sigma-
569 Aldrich) was added at a final concentration of 50 nM. Cells were incubated with 100 µL
570 of each compound at 37 °C with 5% CO₂ for 5 days. A H₂O₂ solution at 10 mM was
571 used as positive control. A HNE solution at 50 nM and culture medium alone were
572 tested as negative controls. MMAE (100 nM, stock solution at 2 µM in PBS) and
573 trastuzumab (100 nM, stock solution at 26 µM in PBS) were used as reference. Cells
574 were incubated with 100 µL of each solution at 37 °C with 5% CO₂ for 5 days. Cell

575 viability was then determined using CellTiter-Glo reagent (Promega, Wiscousin, USA).
576 Briefly, 100 μ L of medium were removed and 100 μ L of CellTiter-Glo reagent were
577 added to each well. The plates were shaken 2 min and then incubated at room
578 temperature for 10 min. The luminescence values were measured with a gain at 135,
579 with an acquisition at 0.5 s, using an absorbance microplate reader (Bio-Tek®
580 instruments, Inc., Vermont, USA). When a dose-dependent activity was observed, 50%
581 inhibitory concentration (IC₅₀) were calculated using Graphpad PRISM 7 software (n =
582 4 in quadruplicate).

583

584 **Acknowledgments**

585

586 This work was supported by the French National Research Agency under the program
587 “Investissements d’avenir” Grant Agreement LabEx MAbImprove (ANR-10-LABX-
588 53-01), Tours University, La Ligue contre le cancer (comities 18, 35, 36, 37, 41, 44, 53,
589 72, 79, 85), the Centre-Val de Loire Region (projects ARD 2020 Biomédicament:
590 MabCHEM and BIOS, and project APR IR 2017) and FEDER (Fonds européen de
591 développement régional). S. Huvelle and S. Henrion thank Centre-Val de Loire Region
592 for their postdoctoral fellowships. I. Ait Mohamed Amar thanks Centre-Val de Loire
593 Region for her PhD fellowship. The authors thank the « *Plateforme Scientifique et*
594 *Technique Analyses des Systèmes Biologiques* » (PST-ASB), Tours (France), for NMR
595 spectrometry. We thank Eloi Haudebourg, Vincent Caulier, and Nicolas Albrecht from
596 the team IMT GICC EA7501 for mass analysis.

597

598

599 **References**

- 600 [1] N. Joubert, A. Beck, C. Dumontet, C. Denevault-Sabourin, Antibody-Drug
601 Conjugates: The Last Decade, *Pharmaceuticals*. 13 (2020) 235.
602 doi:10.3390/ph13090245.
- 603 [2] A. Beck, L. Goetsch, C. Dumontet, N. Corvaia, Strategies and challenges for the
604 next generation of antibody-drug conjugates, *Nat. Rev. Drug Discov.* 16 (2017)
605 315–337. doi:10.1038/nrd.2016.268.
- 606 [3] H. Merten, F. Brandl, A. Plückthun, U. Zangemeister-Wittke, Antibody-Drug

- 607 Conjugates for Tumor Targeting - Novel Conjugation Chemistries and the
608 Promise of non-IgG Binding Proteins, *Bioconjug. Chem.* 26 (2015) 2176–2185.
609 doi:10.1021/acs.bioconjchem.5b00260.
- 610 [4] R.V.J. Chari, M.L. Miller, W.C. Widdison, Antibody-drug conjugates: An
611 emerging concept in cancer therapy, *Angew. Chemie - Int. Ed.* 53 (2014) 3796–
612 3827. doi:10.1002/anie.201307628.
- 613 [5] H. Bouchard, C. Viskov, C. Garcia-Echeverria, Antibody-drug conjugates - A
614 new wave of cancer drugs, *Bioorganic Med. Chem. Lett.* 24 (2014) 5357–5363.
615 doi:10.1016/j.bmcl.2014.10.021.
- 616 [6] U. Hafeez, S. Parakh, H.K. Gan, A.M. Scott, Antibody-drug conjugates for
617 cancer therapy, *Molecules.* 25 (2020) 4764. doi:10.3390/molecules25204764.
- 618 [7] C. Denevault-Sabourin, F. Bryden, M.-C. Viaud-Massuard, N. Joubert,
619 Antibody-drug conjugates: Empowering antibodies for the fight against cancer,
620 *Successful Drug Discovery*, 4 (2019) 55–82. doi:10.1002/9783527814695.ch3.
- 621 [8] H.K. Erickson, P.U. Park, W.C. Widdison, Y. V. Kovtun, L.M. Garrett, K.
622 Hoffman, R.J. Lutz, V.S. Goldmacher, W.A. Blättler, Antibody-maytansinoid
623 conjugates are activated in targeted cancer cells by lysosomal degradation and
624 linker-dependent intracellular processing, *Cancer Res.* 66 (2006) 4426–4433.
625 doi:10.1158/0008-5472.CAN-05-4489.
- 626 [9] Y. V. Kovtun, C.A. Audette, Y. Ye, H. Xie, M.F. Ruberti, S.J. Phinney, B.A.
627 Leece, T. Chittenden, W.A. Blättler, V.S. Goldmacher, Antibody-drug conjugates
628 designed to eradicate tumors with homogeneous and heterogeneous expression of
629 the target antigen, *Cancer Res.* 66 (2006) 3214–3221. doi:10.1158/0008-
630 5472.CAN-05-3973.
- 631 [10] N. Joubert, C. Denevault-Sabourin, F. Bryden, M.-C. Viaud-Massuard, Towards
632 antibody-drug conjugates and prodrug strategies with extracellular stimuli-
633 responsive drug delivery in the tumor microenvironment for cancer therapy, *Eur.*
634 *J. Med. Chem.* 142 (2017) 393–415. doi:10.1016/j.ejmech.2017.08.049.
- 635 [11] M. Barok, H. Joensuu, J. Isola, Trastuzumab emtansine: mechanisms of action
636 and drug resistance, *Breast Cancer Res.* 16 (2014) 3378. doi:10.1186/bcr3621.
- 637 [12] G. Li, J. Guo, B.Q. Shen, D.B. Yadav, M.X. Sliwkowski, L.M. Crocker, J.A.
638 Lacap, G.D.L. Phillips, Mechanisms of acquired resistance to trastuzumab

- 639 emtansine in breast cancer cells, *Mol. Cancer Ther.* 17 (2018) 1441–1453.
640 doi:10.1158/1535-7163.MCT-17-0296.
- 641 [13] F.W. Hunter, H.R. Barker, B. Lipert, F. Rothé, G. Gebhart, M.J. Piccart-Gebhart,
642 C. Sotiriou, S.M.F. Jamieson, Mechanisms of resistance to trastuzumab
643 emtansine (T-DM1) in HER2-positive breast cancer, *Br. J. Cancer.* 122 (2020)
644 603–612. doi:10.1038/s41416-019-0635-y.
- 645 [14] C. Ríos-Luci, S. García-Alonso, E. Díaz-Rodríguez, M. Nadal-Serrano, J.
646 Arribas, A. Ocaña, A. Pandiella, Resistance to the antibody–drug conjugate T-
647 DM1 is based in a reduction in lysosomal proteolytic activity, *Cancer Res.* 77
648 (2017) 4639–4651. doi:10.1158/0008-5472.CAN-16-3127.
- 649 [15] K.J. Hamblett, A.P. Jacob, J.L. Gurgel, M.E. Tometsko, B.M. Rock, S.K. Patel,
650 R.R. Milburn, S. Siu, S.P. Ragan, D.A. Rock, C.J. Borths, J.W.O. Neill, W.S.
651 Chang, M.F. Weidner, M.M. Bio, K.C. Quon, W.C. Fanslow, SLC46A3 Is
652 Required to Transport Catabolites of Noncleavable Antibody Maytansine
653 Conjugates from the Lysosome to the Cytoplasm, *Cancer Res.* 75 (2015) 5329–
654 5340. doi:10.1158/0008-5472.CAN-15-1610.
- 655 [16] J. Sauveur, E.-L. Matera, K. Chettab, P. Valet, J. Guitton, A. Savina, C.
656 Dumontet, Esophageal cancer cells resistant to T-DM1 display alterations in cell
657 adhesion and the prostaglandin pathway, *Oncotarget.* 9 (2018) 21141–21155.
658 doi:10.18632/oncotarget.24975.
- 659 [17] A.H. Staudacher, M.P. Brown, Antibody drug conjugates and bystander killing:
660 is antigen-dependent internalisation required, *Br. J. Cancer.* 117 (2017) 1736–
661 1742. doi:10.1038/bjc.2017.367.
- 662 [18] J.F. DiJoseph, M.M. Dougher, D.C. Armellino, L. Kalyandrug, A. Kunz, E.R.
663 Boghaert, P.R. Hamann, N.K. Damle, CD20-specific antibody-targeted
664 chemotherapy of non-Hodgkin B-cell lymphoma using calicheamicin-conjugated
665 rituximab, *Cancer Immunol. Immunother.* 56 (2007) 1107–1117.
666 doi:10.1007/s00262-006-0260-5.
- 667 [19] R.M. Sharkey, H. Karacay, S. V. Govindan, D.M. Goldenberg, Combination
668 radioimmunotherapy and chemoimmunotherapy involving different or the same
669 targets improves therapy of human pancreatic carcinoma xenograft models, *Mol.*
670 *Cancer Ther.* 10 (2011) 1072–1081. doi:10.1158/1535-7163.MCT-11-0115.

- 671 [20] S. V. Govindan, T.M. Cardillo, S.J. Moon, H.J. Hansen, D.M. Goldenberg,
672 CEACAM5-targeted therapy of human colonic and pancreatic cancer xenografts
673 with potent labetuzumab-SN-38 immunoconjugates, *Clin. Cancer Res.* 15 (2009)
674 6052–6061. doi:10.1158/1078-0432.CCR-09-0586.
- 675 [21] G.J.L. Bernardes, G. Casi, S. Trüssel, I. Hartmann, K. Schwager, J.
676 Scheuermann, D. Neri, A traceless vascular-targeting antibody-drug conjugate
677 for cancer therapy, *Angew. Chemie - Int. Ed.* 51 (2012) 941–944.
678 doi:10.1002/anie.201106527.
- 679 [22] M. Steiner, I. Hartmann, E. Perrino, G. Casi, S. Brighton, I. Jelesarov, G.J.L.
680 Bernardes, D. Neri, Spacer length shapes drug release and therapeutic efficacy of
681 traceless disulfide-linked ADCs targeting the tumor neovasculature, *Chem. Sci.* 4
682 (2013) 297–302. doi:10.1039/c2sc21107f.
- 683 [23] R. Gébleux, M. Stringhini, R. Casanova, A. Soltermann, D. Neri, Non-
684 internalizing antibody-drug conjugates display potent anti-cancer activity upon
685 proteolytic release of monomethyl auristatin E in the subendothelial extracellular
686 matrix, *Int. J. Cancer.* 140 (2017) 1670–1679. doi:10.1002/ijc.30569.
- 687 [24] A.G. Poison, J. Calemine-Fenaux, P. Chan, W. Chang, E. Christensen, S. Clark,
688 F.J. De Sauvage, D. Eaton, K. Elkins, J. Michael Elliott, G. Frantz, R.N. Fuji, A.
689 Gray, K. Harden, G.S. Ingle, N.M. Kljavin, H. Koeppen, C. Nelson, S. Prabhu,
690 H. Raab, S. Ross, J.P. Stephan, S.J. Scales, S.D. Spencer, R. Vandlen, B. Wranik,
691 S.F. Yu, B. Zheng, A. Ebens, Antibody-drug conjugates for the treatment of non-
692 Hodgkin’s lymphoma: Target and linker-drug selection, *Cancer Res.* 69 (2009)
693 2358–2364. doi:10.1158/0008-5472.CAN-08-2250.
- 694 [25] C. Szot, D.S. Dimitrov, B.S. Croix, C. Szot, S. Saha, X.M. Zhang, Z. Zhu, M.B.
695 Hilton, K. Morris, S. Seaman, J.M. Dunleavey, K. Hsu, G. Yu, H. Morris, D.A.
696 Swing, D.C. Haines, Y. Wang, J. Hwang, Y. Feng, D. Welsch, G. Decrescenzo,
697 A. Chaudhary, E. Zudaire, D.S. Dimitrov, B.S. Croix, Tumor stroma-targeted
698 antibody-drug conjugate triggers localized anticancer drug release, 128 (2018)
699 2927–2943. doi: 10.1172/JCI120481.
- 700 [26] S.O. Doronina, B.E. Toki, M.Y. Torgov, B.A. Mendelsohn, C.G. Cerveny, D.F.
701 Chace, R.L. DeBlanc, R.P. Gearing, T.D. Bovee, C.B. Siegall, J.A. Francisco,
702 A.F. Wahl, D.L. Meyer, P.D. Senter, Development of potent monoclonal

703 antibody auristatin conjugates for cancer therapy, *Nat. Biotechnol.* 21 (2003)
704 778–784. doi:10.1038/nbt832.

705 [27] G.M. Dubowchik, R.A. Firestone, L. Padilla, D. Willner, S.J. Hofstead, K.
706 Mosure, J.O. Knipe, S.J. Lasch, P.A. Trail, Cathepsin B-labile dipeptide linkers
707 for lysosomal release of doxorubicin from internalizing immunoconjugates:
708 Model studies of enzymatic drug release and antigen-specific in vitro anticancer
709 activity, *Bioconjug. Chem.* 13 (2002) 855–869. doi:10.1021/bc025536j.

710 [28] H.G. Lerchen, J. Baumgarten, A. Schoop, M. Albers, Enzyme-activated
711 cytostatic conjugates with integrin ligands. PCT/WO 072151, 2002.

712 [29] I. Lerman, S.R. Hammes, Neutrophil elastase in the tumor microenvironment,
713 *Steroids.* 133 (2018) 96–101. doi:10.1016/j.steroids.2017.11.006.

714 [30] A. Raposo Moreira Dias, A. Pina, A. Dean, H.G. Lerchen, M. Caruso, F.
715 Gasparri, I. Fraietta, S. Troiani, D. Arosio, L. Belvisi, L. Pignataro, A. Dal Corso,
716 C. Gennari, Neutrophil Elastase Promotes Linker Cleavage and Paclitaxel
717 Release from an Integrin-Targeted Conjugate, *Chem. - A Eur. J.* 25 (2019) 1696–
718 1700. doi:10.1002/chem.201805447.

719 [31] N. Aubrey, E. Allard-Vannier, C. Martin, F. Bryden, S. Letast, C. Colas, Z.
720 Lakhrif, N. Collinet, I. Dimier-Poisson, I. Chourpa, M.C. Viaud-Massuard, N.
721 Joubert, Site-Specific Conjugation of Auristatins onto Engineered scFv Using
722 Second Generation Maleimide to Target HER2-positive Breast Cancer in Vitro,
723 *Bioconjug. Chem.* 29 (2018) 3516–3521. doi:10.1021/acs.bioconjchem.8b00668.

724 [32] F. Bryden, C. Martin, S. Letast, E. Lles, I. Viéitez-Villemin, A. Rousseau, C.
725 Colas, M. Brachet-Botineau, E. Allard-Vannier, C. Larbouret, M.C. Viaud-
726 Massuard, N. Joubert, Impact of cathepsin B-sensitive triggers and hydrophilic
727 linkers on in vitro efficacy of novel site-specific antibody-drug conjugates, *Org.*
728 *Biomol. Chem.* 16 (2018) 1882–1889. doi:10.1039/c7ob02780j.

729 [33] N. Joubert, C. Martin, G. Brachet, C. Colas, E. Allard-Vannier, C. Kizlik-
730 Masson, C. Esnault, R. Respaud, C. Denevault-Sabourin, I. Chourpa, V.
731 Gouilleux-Gruart, M.C. Viaud-Massuard, In vitro characterization and stability
732 profiles of antibody–fluorophore conjugates derived from interchain cysteine
733 cross-linking or lysine bioconjugation, *Pharmaceuticals.* 12 (2019) 176.
734 doi:10.3390/ph12040176.

- 735 [34] V. Corvaglia, M. Amar, V. Garambois, C. Gongora, M. Del Rio, C. Denevault-
736 sabourin, N. Joubert, I. Huc, P. Pourquier, Internalization of Foldamer-Based
737 DNA Mimics through a Site-Specific Antibody Conjugate to Target HER2-
738 Positive Cancer Cells, *Pharmaceuticals*. 14 (2021) 624.
- 739 [35] F.F. Schumacher, J.P.M. Nunes, A. Maruani, V. Chudasama, M.E.B. Smith, K.A.
740 Chester, J.R. Baker, S. Caddick, Next generation maleimides enable the
741 controlled assembly of antibody-drug conjugates via native disulfide bond
742 bridging, *Org. Biomol. Chem.* 12 (2014) 7261. doi:10.1039/C4OB01550A.
- 743 [36] J.P.M. Nunes, M. Morais, V. Vassileva, E. Robinson, V.S. Rajkumar, M.E.B.
744 Smith, R.B. Pedley, S. Caddick, J.R. Baker, V. Chudasama, Functional native
745 disulfide bridging enables delivery of a potent, stable and targeted antibody-drug
746 conjugate (ADC), *Chem. Commun.* 51 (2015) 10624–10627.
747 doi:10.1039/C5CC03557K.
- 748 [37] G. Badescu, P. Bryant, M. Bird, K. Henseleit, J. Swierkosz, V. Parekh, R.
749 Tommasi, E. Pawlisz, K. Jurlewicz, M. Farys, N. Camper, X. Sheng, M. Fisher,
750 R. Grygorash, A. Kyle, A. Abhilash, M. Frigerio, J. Edwards, A. Godwin,
751 Bridging disulfides for stable and defined antibody drug conjugates, *Bioconjug.*
752 *Chem.* 25 (2014) 1124–1136. doi:10.1021/bc500148x.
- 753 [38] C.R. Behrens, E.H. Ha, L.L. Chinn, S. Bowers, G. Probst, M. Fitch-Bruhns, J.
754 Monteon, A. Valdiosera, A. Bermudez, S. Liao-Chan, T. Wong, J. Melnick, J.W.
755 Theunissen, M.R. Flory, D. Houser, K. Venstrom, Z. Levashova, P. Sauer, T.S.
756 Migone, E.H. Van Der Horst, R.L. Halcomb, D.Y. Jackson, Antibody-Drug
757 Conjugates (ADCs) Derived from Interchain Cysteine Cross-Linking
758 Demonstrate Improved Homogeneity and Other Pharmacological Properties over
759 Conventional Heterogeneous ADCs, *Mol. Pharm.* 12 (2015) 3986–3998.
760 doi:10.1021/acs.molpharmaceut.5b00432.
- 761 [39] K.J. Hamblett, P.D. Senter, D.F. Chace, M.M.C. Sun, J. Lenox, C.G. Cervený,
762 K.M. Kissler, S.X. Bernhardt, A.K. Kopcha, R.F. Zabinski, D.L. Meyer, J.A.
763 Francisco, Effects of drug loading on the antitumor activity of a monoclonal
764 antibody drug conjugate, *Clin. Cancer Res.* 10 (2004) 7063–7070.
765 doi:10.1158/1078-0432.CCR-04-0789.
- 766 [40] M.M.C. Sun, K.S. Beam, C.G. Cervený, K.J. Hamblett, R.S. Blackmore, M.Y.

767 Torgov, F.G.M. Handley, N.C. Ihle, P.D. Senter, S.C. Alley, Reduction-
768 alkylation strategies for the modification of specific monoclonal antibody
769 bisulfides, *Bioconjug. Chem.* 16 (2005) 1282–1290. doi:10.1021/bc050201y.

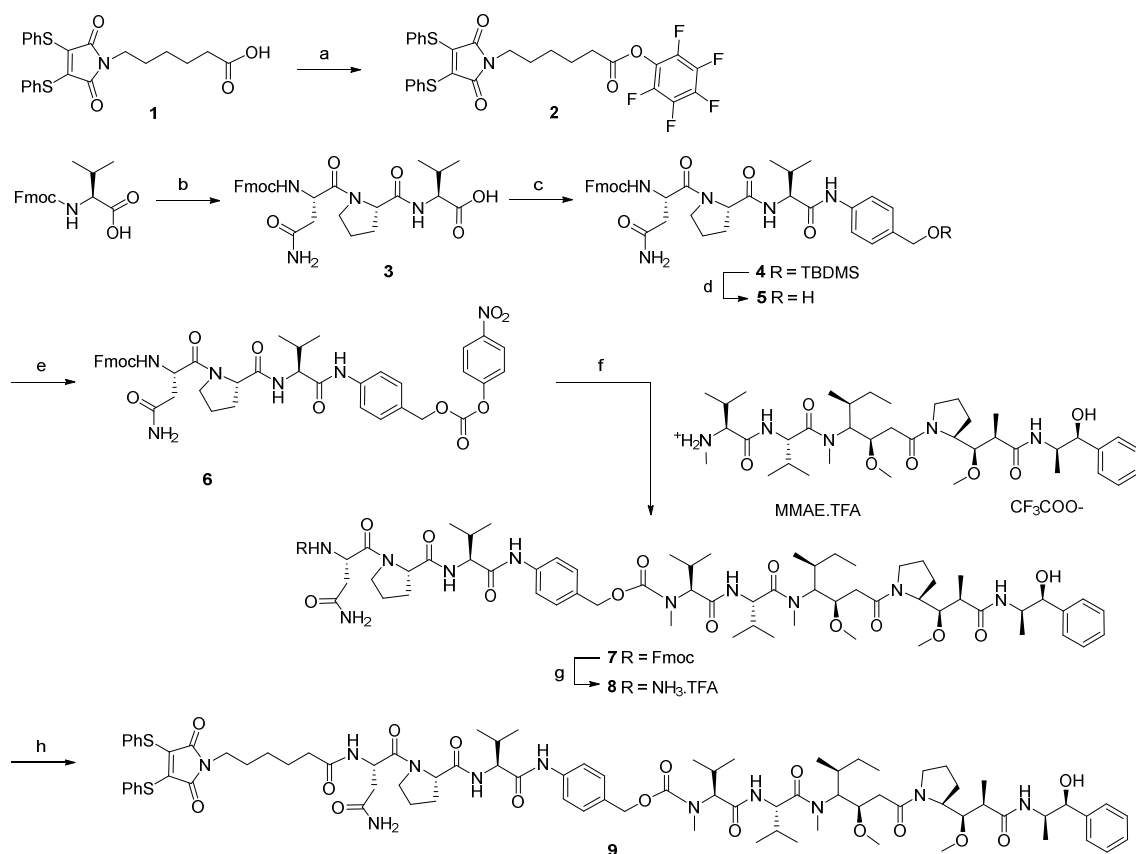
770 [41] S.P.M. Crouch, R. Kozlowski, K.J. Slater, J. Fletcher, The use of ATP
771 bioluminescence as a measure of cell proliferation and cytotoxicity, *160* (1993)
772 81–88.

773 [42] D. Hanahan, R.A. Weinberg, Hallmarks of cancer: The next generation, *Cell.* 144
774 (2011) 646–674. doi:10.1016/j.cell.2011.02.013.

775 [43] K.M. Haynes, N. Abdali, V. Jhawar, H.I. Zgurskaya, J.M. Parks, A.T. Green, J.
776 Baudry, V. V. Rybenkov, J.C. Smith, J.K. Walker, Identification and Structure-
777 Activity Relationships of Novel Compounds that Potentiate the Activities of
778 Antibiotics in *Escherichia coli*, *J. Med. Chem.* 60 (2017) 6205–6219.
779 doi:10.1021/acs.jmedchem.7b00453.

780

781

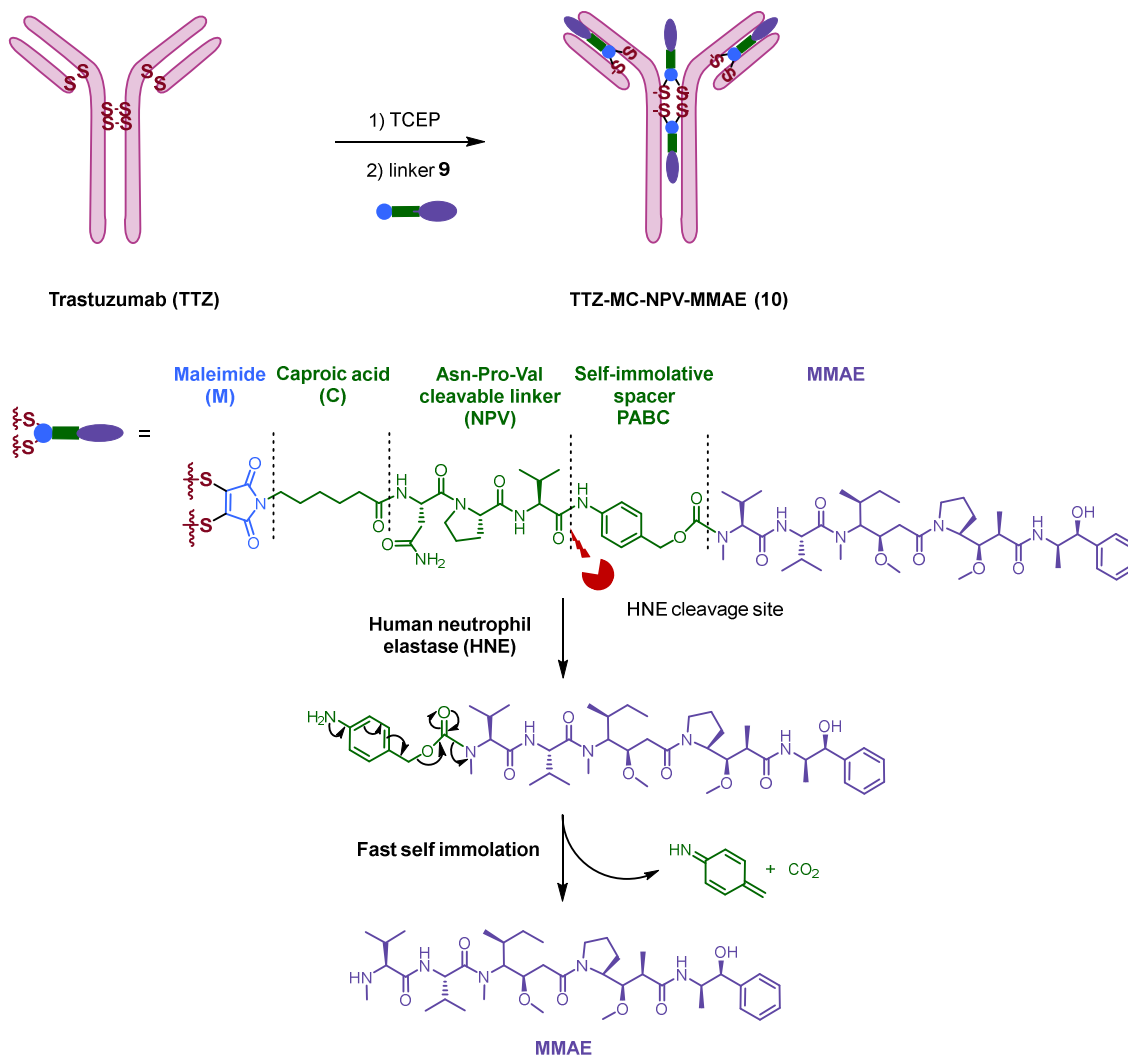


782
783

784 **Scheme 1.** Reagents and conditions: (a) **1** (1 eq), pentafluorophenol (1 eq), *N,N'*-
785 dicyclohexylcarbodiimide (DCC) (1 eq), THF, 0 °C, and then rt, overnight, 91%; (b) 1)
786 Fmoc-Pro-OH (4 eq), diisopropylcarbodiimide (DIC) (4 eq), Oxyma (4 eq), DMF, *N*-
787 methyl-2-pyrrolidone, 70 °C, 30 min, 2) Fmoc-Asn(Trt)-OH (1.5 eq), DIC (4 eq),
788 Oxyma (4 eq), DMF, *N*-methyl-2-pyrrolidone, 70 °C, 30 min, 3) TFA/H₂O/TIPS,
789 MeOH, rt, 2 h, 82%; (c) 1) DCC (1.5 eq), 4-dimethylaminopyridine (cat.), DCM, 0 °C,
790 1 h, 2) 4-(((*tert*-butyldimethylsilyl)oxy)methyl)aniline (1 eq), rt, overnight, 60%; (d)
791 HCl (37%), EtOH, rt, 2 h, 92%; (e) *para*-nitrophenyl chloroformate (2 eq), pyridine (2.5
792 eq), THF, rt, overnight, 96%; (f) MMAE TFA salt (0.67 eq), hydroxybenzotriazole
793 (HOBt) (3.3 eq), *N,N'*-diisopropylethylamine (DIPEA) (2 eq), DMF, rt, overnight, 48%;
794 (g) Piperidine (20%), DMF, rt, 1 h, then (h) **2** (1 eq), HOBt (2 eq), DIPEA (2.2 eq),
795 DMF, rt, overnight, 30% over two steps.

796

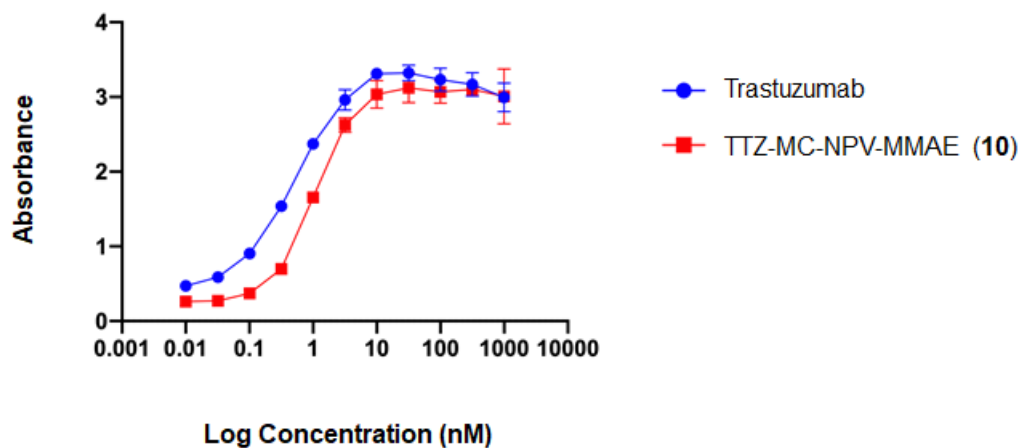
797



798

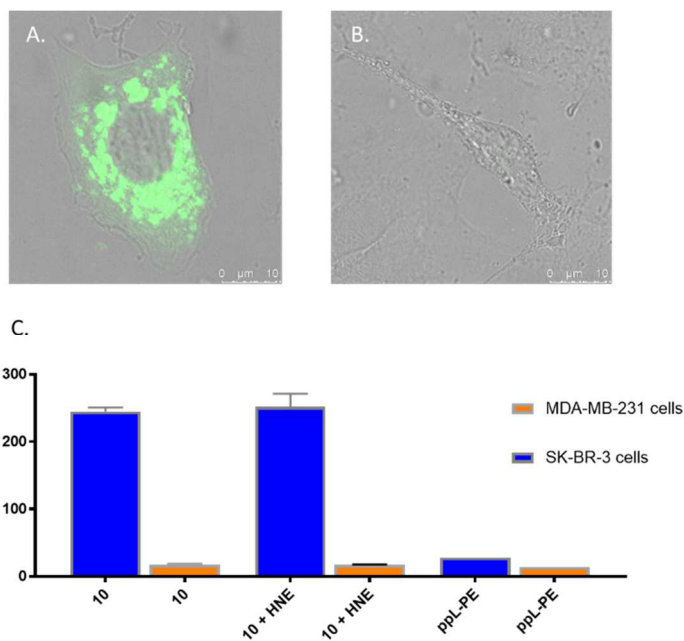
799 **Fig. 1.** Bioconjugation process, structure, and mechanism of MMAE release of the
 800 TTZ-MC-NPV-MMAE (10).

801



802
803
804
805
806
807

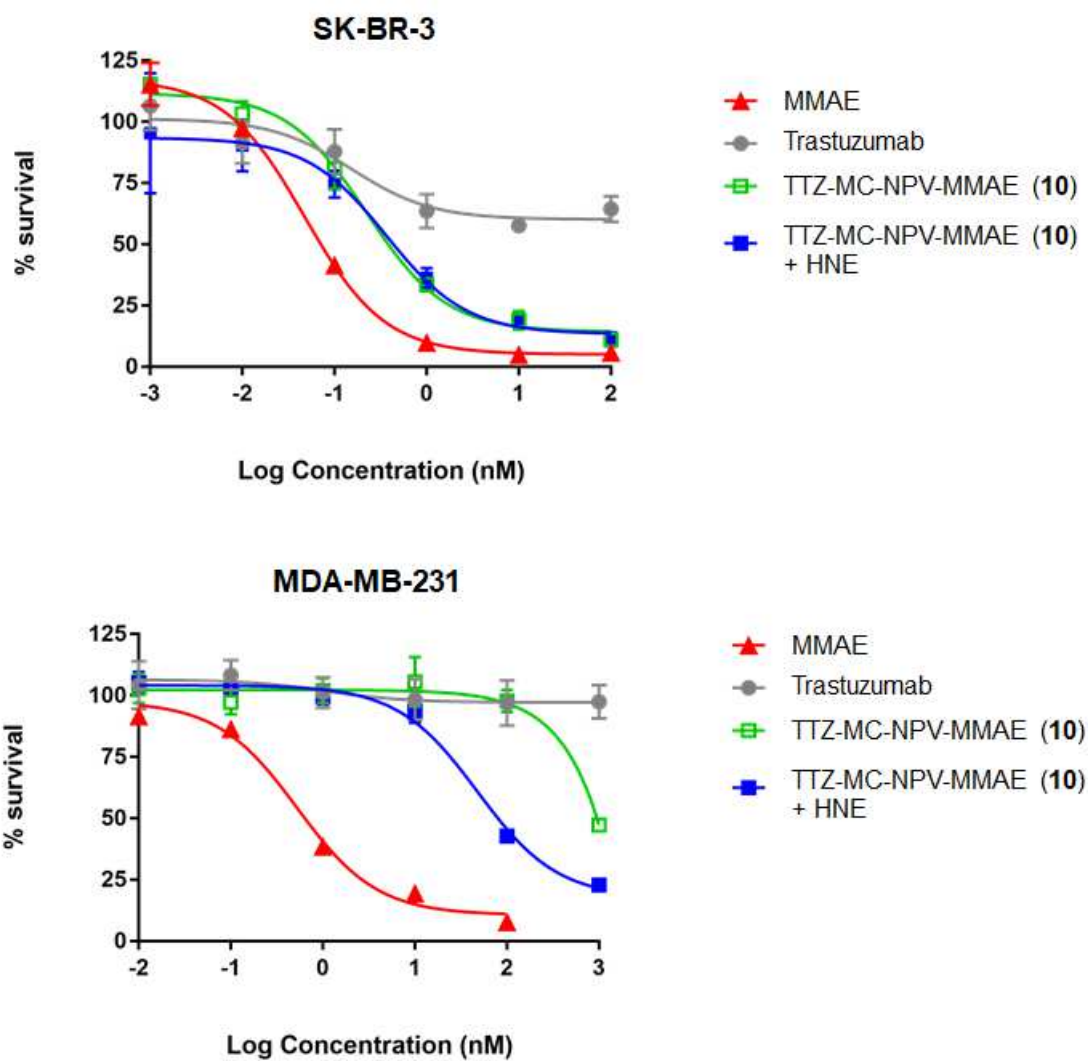
Fig. 2. HER2 binding affinities of TTZ-MC-NPV-MMAE (**10**) (red curve) in comparison to trastuzumab (blue curve) determined by ELISA.



808
809
810
811
812
813
814

Fig. 3. Confocal microscopy images of SK-BR-3 (HER2+) (A) and MDA-MB-231 (HER2-) (B) cell lines after exposure to TTZ-MC-NPV-MMAE (**10**) for 48 h. (C) Internalization of ADC **10** after complexation with ppl-PE in SK-BR-3 and MDA-MB-231 cell lines, as analyzed by flow cytometry (exposure time = 48 h).

815



816

817 **Fig. 4.** *In vitro* cytotoxic activity of TTZ-MC-NPV-MMAE (10) in comparison to
818 trastuzumab and free MMAE on SK-BR-3 and MDA-MB-231 cancer cell lines.

819

820 **Table 1**821 Cell-based assays of TTZ-MC-NPV-MMAE (**10**) with or without HNE.

Entry	Compd	IC ₅₀ (nM) ^a	
		SK-BR-3 (HER2+) ^b	MDA-MB-231 (HER2-) ^b
1	ADC 10	0.23 ± 0.08	> 1000
2	ADC 10 + HNE ^c	0.36 ± 0.13	47.5 ± 7.9
3	Trastuzumab	> 1000	> 1000
4	MMAE	0.05 ± 0.01	0.53 ± 0.06

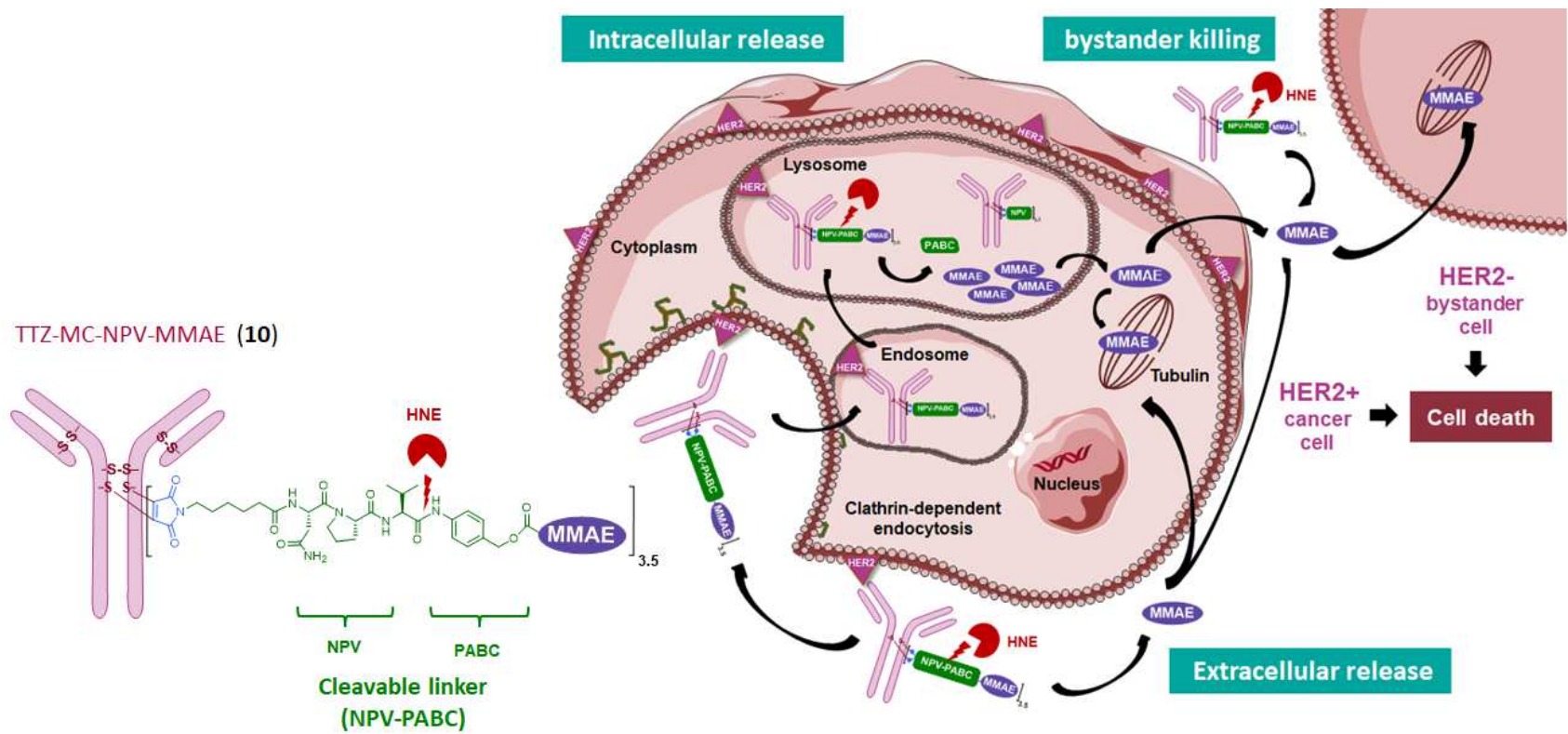
822

823 ^a IC₅₀ were calculated from dose-response curves. Each compound concentration was tested in
824 quadruplicate.825 ^b Cells were treated for 5 days, with concentrations ranging from 0.01 to 1000 nM for MDA-MB-231
826 cells and from 0.001 to 100 nM for SK-BR-3 cells. Cell viability was determined by quantification of
827 ATP, using the CellTiter-Glo cell proliferation assay, and IC₅₀ values were calculated using
828 Graphpad PRISM 7 software (n = 4 in quadruplicate).829 ^c HNE enzyme was added at a final concentration of 50 nM, concentration at which HNE had a
830 negligible effect on cell viability alone.

831

832

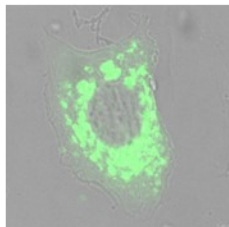
833



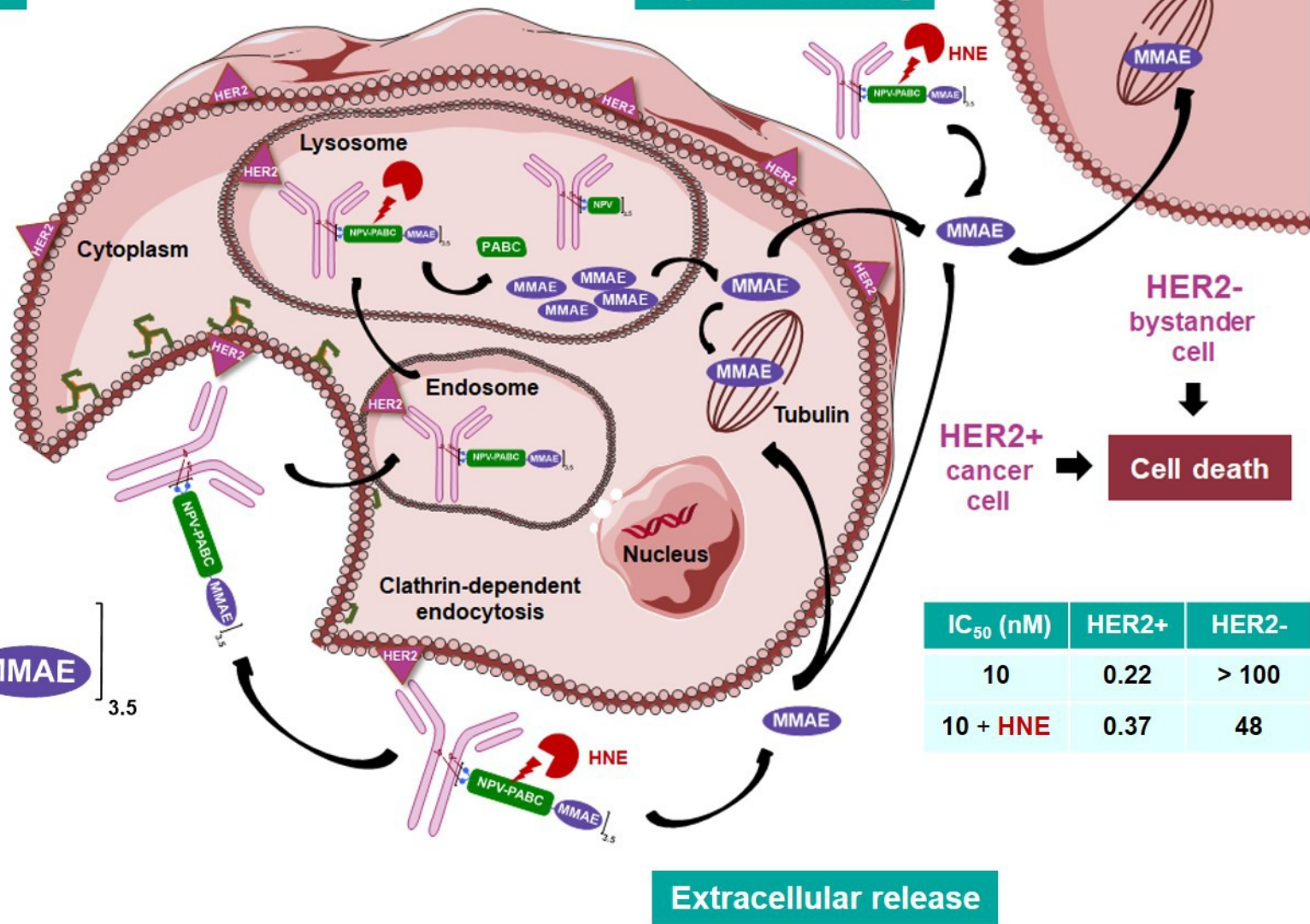
834
 835
 836
 837
 838
 839

Fig. 5. Proposed mechanism of action for TTZ-MC-NPV-MMAE (10).

Intracellular release



bystander killing



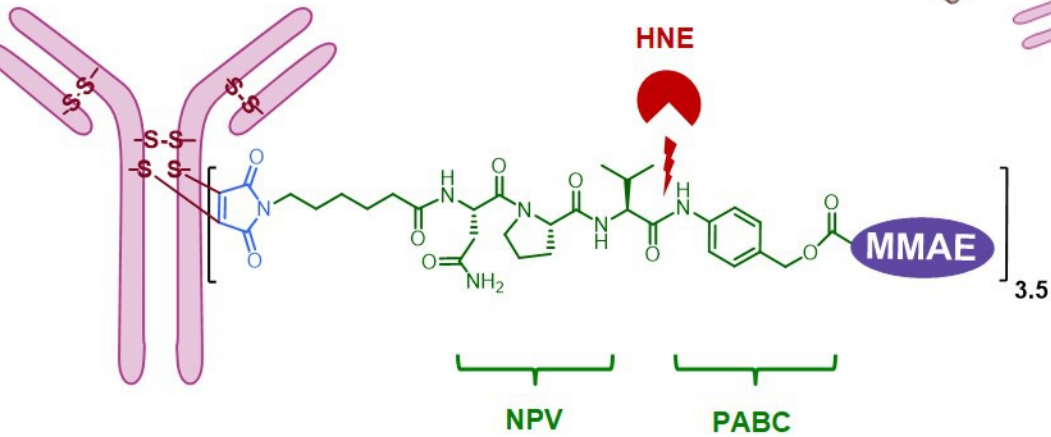
HER2-
bystander
cell

Cell death

IC ₅₀ (nM)	HER2+	HER2-
10	0.22	> 100
10 + HNE	0.37	48

Extracellular release

TTZ-MC-NPV-MMAE (10)



Cleavable linker
(NPV-PABC)